Effect of Ultra-High-Resolution CT on Pseudoenhancement in Renal Cysts: A Phantom Experiment and Clinical Study

Fumiko Hamabe, MD[1], Ayako Mikoshi, MD[1], Hiromi Edo, MD, PhD[1], Hiroaki Sugiura, MD, PhD[1], Kousuke Okano, MD[1], Yoshitake Yamada, MD, PhD[2], Masahiro Jinzaki, MD, PhD[2], Hiroshi Shinmoto, MD, PhD[1]

Genitourinary Imaging · Original Research

Keywords

cystic, diagnostic imaging, image enhancement, kidney diseases, MDCT

Submitted: Jan 7, 2022
Revision requested: Jan 20, 2022
Revision received: Feb 15, 2022
Accepted: May 9, 2022
First published online: May 18, 2022

The authors declare that there are no disclosures relevant to the subject matter of this article.

Supported in part by Keio Gijuku Academic Development Funds for the creation of the phantom design.

An electronic supplement is available online at doi.org/10.2214/AJR.22.27354.

BACKGROUND. Ultra-high-resolution CT (UHRCT) allows acquisition using a small detector element size, in turn allowing very high spatial resolutions. The high resolution may reduce partial-volume averaging and thereby renal cyst pseudoenhancement.

OBJECTIVE. The purpose of this article was to assess the impact of UHRCT on renal cyst pseudoenhancement.

METHODS. A phantom was constructed that contained 7-, 15-, and 25-mm simulated cysts within compartments simulating unenhanced and nephrographic phase renal parenchyma. The phantom underwent two UHRCT acquisitions using 0.25- and 0.5-mm detector elements, with reconstruction at varying matrices and slice thicknesses. A retrospective study was performed of 36 patients (24 men, 12 women; mean age, 75.7 ± 9.4 [SD] years) with 118 renal cysts who underwent renal-mass protocol CT using UHRCT and the 0.25-mm detector element, with reconstruction at varying matrices and slice thicknesses; detector element size could not be retrospectively adjusted. ROIs were placed to measure cysts' attenuation increase from unenhanced to nephrographic phases (to reflect pseudoenhancement) and SD of unenhanced phase attenuation (to reflect image noise).

RESULTS. In the phantom, attenuation increase was lower for the 0.25- than 0.5-mm detector element for the 15-mm cyst (4.6 ± 2.7 HU vs 6.8 ± 2.9 HU, $p = .03$) and 25-mm cyst (2.3 ± 1.4 HU vs 3.8 ± 1.2 HU, $p = .02$), but not the 7-mm cyst ($p = .72$). Attenuation increase was not different between 512 × 512 and 1024 × 1024 matrices for any cyst size in the phantom or patients ($p > .05$). Attenuation increase was not associated with slice thickness for any cyst size in the phantom or in patients for cysts that were between 5 mm and less than 10 mm and those that were 10 mm and larger ($p > .05$). For cysts smaller than 5 mm in patients, attenuation increase showed decreases with thinner slices, though there was no significant difference between 0.5-mm and 0.25-mm (3-mm slice: 23.7 ± 22.5 HU; 2-mm slice: 20.2 ± 22.7 HU; 0.5-mm slice: 11.6 ± 17.5 HU; 0.25-mm slice: 12.6 ± 19.7 HU; $p < .001$). Smaller detector element size, increased matrix size, and thinner slices all increased image noise for cysts of all sizes in the phantom and patients ($p < .05$).

CONCLUSION. UHRCT may reduce renal cyst pseudoenhancement through a smaller detector element size and, for cysts smaller than 5 mm, very thin slices; however, these adjustments result in increased noise.

CLINICAL IMPACT. Although requiring further clinical evaluation, UHRCT may facilitate characterization of small cystic renal lesions, thereby reducing equivocal interpretations and follow-up recommendations.

The widespread use of CT, along with advances in CT technology, have increased the incidental detection of renal masses, leading to a need for reliable differentiation between renal cysts and neoplasms. Conventional MDCT has been used to characterize renal masses measuring as small as 5–10 mm as cysts [1]. To minimize partial-volume effect when characterizing renal lesions by MDCT, it is recommended to use thin collimation and a reconstructed slice thickness of less than half the size of the lesion being evaluated [1–5].

A recognized pitfall in characterizing small renal lesions as cysts by MDCT is pseudoenhancement, defined as an artifactual increase in attenuation of a renal cyst by 10 to approximately 20 HU [2, 6, 7]. Pseudoenhancement is generally considered to be a result of inadequate correction of beam-hardening artifact by the reconstruction algorithm as a result of enhancement of the renal parenchyma adjacent to the cyst [8–10]. Pseudoenhance-

[1]Department of Radiology, National Defense Medical College, Namiki 3-2, Tokorozawa, Saitama 359-8513, Japan. Address correspondence to H. Shinmoto (hshinmoto@gmail.com).

[2]Department of Radiology, Keio University School of Medicine, Tokyo, Japan.

doi.org/10.2214/AJR.22.27354
AJR 2022; 219:624–633
ISSN-L 0361–803X/22/2194–624

ment is more common in cysts that are small and endophytic [11, 12]. The phenomenon has been shown to vary among CT systems from different manufacturers and from different equipment generations [7, 13] and to be influenced by a range of CT parameters (Table S1, available in the online supplement). Although pseudoenhancement is more severe when using thicker slices because of more pronounced volume averaging, pseudoenhancement itself is a distinct artifact from partial-volume averaging and has been observed even when partial-volume averaging has been minimized [8]. Pseudoenhancement may lead to additional follow-up imaging of incidental renal masses and possible misdiagnosis as a benign cyst.

Ultra-high-resolution CT (UHRCT) has been clinically available since 2017 and provides greatly improved spatial resolution compared with conventional MDCT because of the use of a smaller detector element size, smaller focus size, and larger matrices [14–16]. Specifically, UHRCT uses reconstruction matrix sizes of 1024 × 1024 or 2048 × 2048 compared with 512 × 512 for conventional MDCT and achieves a spatial resolution of 0.12 mm compared with a spatial resolution ranging from 0.23 to 0.35 mm for conventional MDCT [15]. Hata et al. [16] achieved the highest image quality in cadaveric lungs imaged by UHRCT when using a 2048 × 2048 matrix to obtain maximal spatial resolution.

The improved spatial resolution resulting from UHRCT is expected to reduce partial-volume averaging and thus contribute to a decrease in renal cyst pseudoenhancement. On the other hand, the smaller detector element size, larger matrix size, and thinner slices of UHRCT decrease incident photons, thereby increasing image noise and lowering image quality [16–19]. The decrease in incident photons could affect attenuation measurements, resulting in an unclear impact on pseudoenhancement (which could be exacerbated or mitigated). To our knowledge, the impact of UHRCT on renal cyst pseudoenhancement has not been previously investigated. The aim of this study was thus to assess the impact of UHRCT on renal cyst pseudoenhancement, with attention to small (i.e., < 10 mm) cysts.

Methods

This single-center retrospective study adhered to the principles of the Declaration of Helsinki. Approval for the clinical portion was granted by the National Defense Medical College's ethics committee. The requirement for written informed patient consent was waived by the institutional review board.

UHRCT Scanner

A UHRCT scanner (Aquilion Precision, Canon Medical Systems) was used for both a phantom experiment and a clinical study. The UHRCT scanner provides two scan modes: normal-resolution (NR) mode and super-high-resolution (SHR) mode. The NR mode is comparable to conventional CT, is acquired using 896 detector channels and a 0.5-mm detector element, and is reconstructed using a 512 × 512 matrix size. The SHR mode is acquired using 1792 detector channels and a 0.25-mm detector element and can be reconstructed from a single acquisition at a matrix size of either 512 × 512 or 1024 × 1024. Both NR and SHR acquisitions can be reconstructed at different slice thicknesses.

HIGHLIGHTS

Key Finding

- *Using UHRCT, renal cyst pseudoenhancement was decreased in the phantom by using a smaller detector element size of 0.25 mm for the 25- and 15-mm cysts and in patients by decreasing slice thickness to 0.25 or 0.5 mm for cysts smaller than 5 mm; increased matrix size did not reduce pseudoenhancement.*

Importance

- *By enabling very high spatial resolution beyond the resolution of conventional MDCT, UHRCT may reduce partial-volume averaging and thereby reduce pseudoenhancement for small renal cysts.*

Phantom Study

Phantom design—Different materials were used to represent cysts, renal parenchyma, and the abdominal cavity. Three hollow polypropylene spheres measuring 7, 15, and 25 mm in diameter were filled with water (CT attenuation, 0 HU) to simulate simple renal cysts [6, 20]. These were inserted into the center of a polyethylene cylindric kidney phantom to create susceptibility to pseudoenhancement [21]. The kidney phantom had a diameter of 55 mm, matching the mean kidney diameter in an earlier study [21]. Two kidney phantoms were prepared. In one kidney phantom (hereafter, the unenhanced phantom), the space around the spheres was filled with water to simulate unenhanced renal parenchyma. In the other kidney phantom (hereafter, the nephrographic phase phantom), the space around the spheres was filled with contrast agent (ioversol, Optiray 350, Guerbet Japan) diluted with water to yield an attenuation of 174–177 HU; this attenuation reflected the mean attenuation of renal parenchyma in the nephrographic phase on UHRCT according to an initial exploratory evaluation of patients not included in the current study. A pipette was used to remove residual air from the spheres and cylinders. The two kidney phantoms were both inserted into a water-filled body phantom (National Electrical Manufacturers Association) with a lateral dimension of 320 mm, anteroposterior dimension of 220 mm, and height of 200 mm to simulate the human abdominal cavity.

CT technique—The body phantom containing the two kidney phantoms was scanned by UHRCT. The phantom was positioned at the gantry's isocenter, perpendicular to the scanner's *z*-axis. The phantom underwent an acquisition in NR mode, from which image sets at different slice thicknesses were reconstructed, and an acquisition in SHR mode, from which image sets at different matrix sizes were reconstructed. Scan parameters are shown in Table S2 (available in the online supplement). The phantom was imaged 10 times in each mode, and 10 image sets were reconstructed for each combination of detector element size, matrix size, and slice thickness. All reconstructions were performed using hybrid iterative reconstruction.

Experiments—To assess the effect of detector element size, the separate acquisitions using a 0.25-mm detector element (SHR

mode) and a 0.5-mm detector element (NR mode) were both reconstructed using a 512 × 512 matrix and 3-mm slice thickness. To assess the effect of matrix size, the acquisition using a 0.25-mm detector element (SHR mode) was reconstructed at 3-mm slice thickness using both 512 × 512 and 1024 × 1024 matrices. To assess the impact of slice thickness, the acquisition using a 0.25-mm detector element (SHR mode) was reconstructed using a 512 × 512 matrix at slice thicknesses of 0.25, 0.5, 2, 3, and 5 mm. Because of overlap of some reconstructions between these comparisons, a total of seven unique reconstructed image sets were generated.

Image analysis—Two board-certified radiologists (K.O. and H. Shinmoto, with 2 and 31 years of posttraining experience in abdominal CT) independently performed all measurements using PACS (EV Insite R, PSP). The radiologists placed a circular ROI on a single slice corresponding with the *z*-axis center of each of the three simulated renal cysts (7, 15, and 25 mm) for both the unenhanced and nephrographic phase phantoms [22, 23]. The size of the ROI was approximately half of the cyst diameter to minimize partial-volume effects [24, 25]. After placing the ROI in the first image set, the copy-and-paste function was used to transfer the ROIs for the three cysts for both phantoms to all other image sets (i.e., all 10 reconstructions for all seven unique parameter combinations). The mean attenuation of each ROI was recorded, as well as the SD of each ROI for the unenhanced phantom. For each cyst for each of the seven unique parameter combinations, the mean increase in attenuation between the unenhanced and nephrographic phase phantoms for the 10 acquisitions was determined. In addition, for each cyst for each unique parameter combination, the mean SD of the unenhanced phantom for the 10 acquisitions was computed as a measure of image noise.

Clinical Study

Patients and renal cysts—Patient selection was performed by a board-certified radiologist (H.E.) with 7 years of posttraining experience in abdominal imaging who was not involved in subsequent data collection or analysis. The electronic medical record was searched for patients 20 years or older who underwent a clinically indicated CT examination using a multiphase renal-mass protocol that was performed by UHRCT between June 2020 and September 2021, identifying 107 patients. Of these patients, 48 were excluded because the clinical CT report did not describe the presence of any renal cysts. In the remaining patients, the images were reviewed to evaluate all cystic-appearing renal lesions (including those identified on retrospective image review that were not specifically mentioned in the clinical report). On the basis of this review, the cystic-appearing lesions on CT were deemed to represent renal cysts if also having a cystic appearance on either ultrasound or MRI (whether performed with or without IV contrast material) obtained within 36 months before or after the CT and if showing a minimum of 12-month stability according to comparisons with prior and/or subsequent imaging [23, 26]. On the basis of this review, 22 patients were excluded because they did not have at least one renal lesion meeting these criteria for simple renal cysts, and one patient was excluded because of polycystic kidney disease. After these exclusions, the clinical study included 36 patients (24 men, 12 women; mean age, 75.7 ± 9.4 years; age range, 54–92 years) with 118 simple renal cysts (60 in the right kidney, 58 in the left kidney; mean cyst diameter, 10.8 ± 11.7 mm; cyst diameter range, 1.2–102.1 mm). Figure 1 summarizes the flow of patient selection. Patients' height and weight were retrieved from medical records and used to calculate BMI.

CT technique—Patients underwent multiphase contrast-enhanced renal-mass protocol CT using the UHRCT scanner. After acquiring the anterior digital scout radiograph, unenhanced images were obtained from the top of the kidneys through the urinary bladder. Patients then received nonionic contrast medium (ioversol) at 600 mg I/kg of iodine via a dual-head power injector through a vein in the antecubital fossa, with an injection duration of 30 seconds. Contrast-enhanced phases included arterial, corticomedullary, nephrographic, and delayed phases for the kidneys. The scan delay for the arterial phase was estimated according to automatic bolus tracking with the ROI placed in the abdominal aorta at the level of the celiac trunk. The arterial phase acquisition was started once the contrast enhancement in the ROI reached 150 HU. The corticomedullary, nephrographic, and delayed phases were acquired at 35, 90, and 150 seconds after the start of IV contrast medium injection.

Unenhanced images and enhanced images in all four phases were acquired in SHR mode, from which image sets at different matrix sizes and slice thicknesses were reconstructed. No acqui-

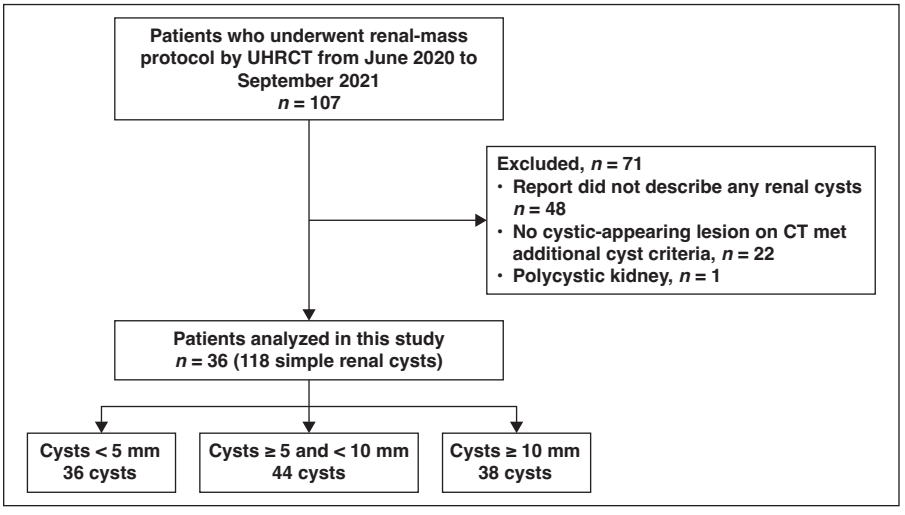

Fig. 1—Illustration shows patient flowchart. Additional criteria for renal cysts included cystic appearance on ultrasound or MRI and minimum of 12-month stability on basis of prior and/or subsequent imaging. UHRCT = ultra-high-resolution CT.

sitions in NR mode were obtained. Aside from not obtaining an NR-mode acquisition, scanning parameters were comparable to those used in the phantom study (Table S2). All images were reconstructed using hybrid iterative reconstruction.

Experiments—The effect of detector element size could not be evaluated in the clinical study because only an SHR-mode acquisition was obtained; the SHR-mode acquisition uses a 0.25-mm detector element size and cannot be retrospectively reconstructed to reflect a different detector element size. To assess the effect of matrix size, the single unenhanced and nephrographic phase acquisitions (both in SHR mode using a 0.25-mm detector element size) were reconstructed at 3-mm slice thickness using both 512 × 512 and 1024 × 1024 matrix sizes. To assess the effect of slice thickness, the single unenhanced and nephrographic phase acquisitions (both in SHR mode using a 0.25-mm detector element) were reconstructed using a 512 × 512 matrix at slice thicknesses of 0.25, 0.5, 2, 3, and 5 mm. Because of overlap of some reconstructions between these comparisons, a total of six unique reconstructed image sets were generated for each phase.

Image analysis—Two board-certified radiologists (A.M. and H. Sugiura, with 3 and 20 years of posttraining experience in abdominal CT) independently performed all measurements using PACS. The radiologists placed a circular or ovoid ROI on each renal cyst. The size of the ROI was approximately half of the cyst diameter [24, 25]. The ROI position was manually adjusted if the cyst's position shifted between the unenhanced and nephrographic phase images because of variation in the patient's breath-holding or other patient motion. The default abdominal window setting (width, 400 HU; level, 40 HU) was used for the ROI measurements.

The ROIs placed on the unenhanced and nephrographic phase images for each cyst were transferred using the copy-and-paste function to all other image sets (i.e., all six unique parameter reconstructions). The mean attenuation of each ROI was recorded, as well as the SD of each ROI for the unenhanced phase. Cysts were stratified into three groups according to size (< 5 mm, ≥ 5 to < 10 mm, ≥ 10 mm). For each of the six unique parameter combinations for each cyst size range, the mean increase in attenuation between the unenhanced and nephrographic phase images was determined. In addition, for each of the six unique parameter combinations for each cyst size range, the mean SD of the unenhanced phase was computed as a measure of image noise. Finally, for each unique parameter combination for each cyst size range, the percentage of cysts within the size range that demonstrated an attenuation increase of 10 HU and greater, 15 HU and greater, and 20 HU and greater was computed as a measure of pseudoenhancement at various thresholds.

Statistical Analyses

Bland-Altman analyses were used to assess interreader agreement of measurement attenuation increase between unenhanced and nephrographic phase images for each unique parameter combination for both the phantom experiment and clinical studies. For the phantom experiment, the Bland-Altman analysis pooled measurements from the 10 separate acquisitions for three simulated cysts (i.e., 30 measurements per reader) for each unique parameter combination. For the clinical study, the Bland-Altman analysis pooled measurements for all cysts in the study sample (i.e., 118 measurements per reader) for each unique parameter combination. After assessing interreader agreement, mean measurements from the two readers were used for all further analyses.

For the phantom study, Wilcoxon signed rank and Friedman tests were used to compare mean attenuation increase and mean image noise between image sets acquired with detector element sizes of 0.25 and 0.5 mm, between image sets reconstructed with matrix sizes of 512 × 512 and 1024 × 1024, and between image sets reconstructed with slice thicknesses of 0.25, 0.5, 2, 3, and 5 mm. Pairwise comparisons of slice thickness were performed using the Wilcoxon signed rank test. For the clinical study, given the presence of multiple cysts per patient, a linear mixed-effects model analysis was used to compare mean attenuation increase and mean image noise between image sets reconstructed with matrix sizes of 512 × 512 and 1024 × 1024, and between image sets reconstructed with slice thicknesses of 0.25, 0.5, 2, 3, and 5 mm. In the model, the fixed factor was the reconstruction parameter (one of two matrix sizes or one of five slice thicknesses) and the random factor was the patient. Pairwise comparisons of slice thickness were performed using a linear mixed-effects model. The frequencies of an attenuation increase of 10 HU and greater, 15 HU and greater, and 20 HU and greater was computed for each cyst size range and summarized descriptively. Evaluation was not performed in the phantom experiment for the 7-mm cyst for the reconstruction using a 5-mm slice thickness and was not performed in the clinical study for cysts smaller than 5 mm or for those between 5 mm and less than 10 mm for the reconstructions using a 5-mm slice thickness because of anticipated marked partial-volume effect for these assessments, resulting in unreliable attenuation measurements. A p value less than .05 was considered statistically significant. All analyses were performed using the Statistical Package for the Social Sciences (version 24.0, IBM Japan).

Results

Phantom Study

Figure S1 (available in the online supplement) shows the Bland-Altman plots for assessing interreader agreement for the mean attenuation increase for each unique combination of parameters in the phantom experiment. The mean difference between readers for attenuation increase was –1.6 HU for a detector element size, matrix size, and slice thickness of 0.25 mm, 512 × 512, and 0.25 mm; –3.4 HU for 0.25 mm, 512 × 512, and 0.5 mm; 0.5 HU for 0.25 mm, 512 × 512, and 2 mm; –0.6 HU for 0.25 mm, 512 × 512, and 3 mm; 0.6 HU for 0.25 mm, 512 × 512 mm, and 5 mm; –0.5 HU for 0.5 mm, 512 × 512, and 3 mm; and 0.3 HU for 0.25 mm, 1024 × 1024, and 3 mm. Figure 2 shows CT images of the phantom, and Figure 3 shows sample ROI measurements.

Detector element size—Table 1 summarizes the comparisons between detector element sizes in the phantom experiment. The attenuation increase was significantly lower for a detector element size of 0.25 mm than of 0.5 mm for the 15-mm cyst (4.6 ± 2.7 HU vs 6.8 ± 2.9 HU, p = .03) and 25-mm cyst (2.3 ± 1.4 HU vs 3.8 ± 1.2 HU, p = .02), but not for the 7-mm cyst (4.4 ± 4.1 HU vs 5.3 ± 2.7 HU, p = .72). Image noise was significantly greater at a detector element size of 0.25 mm than of 0.5 mm for the 7-mm cyst (13.2 ± 2.6 HU vs 8.5 ± 1.5 HU, p = .005), 15-mm cyst (14.2 ± 2.6 HU vs 8.8 ± 1.3 HU, p = .005), and 25-mm cyst (14.4 ± 0.4 HU vs 9.1 ± 1.2 HU, p = .005).

Matrix size—Table 2 summarizes the comparisons between matrix sizes in the phantom experiment. The attenuation increase

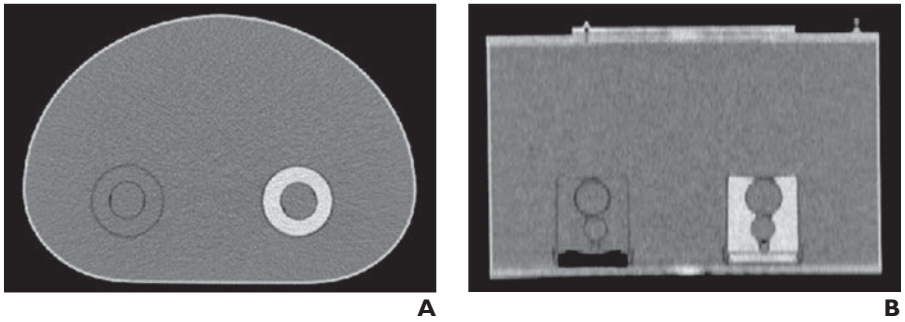

Fig. 2—Ultra-high-resolution CT (UHRCT) images of phantom using 0.25-mm detector element, 512 × 512 matrix, and 3-mm slice thickness.
A and **B,** Axial (**A**) and coronal (**B**) UHRCT views of phantom show outer compartment that corresponds with body, two rectangular middle compartments that correspond with kidneys, and three circular inner compartments within each middle compartment that correspond with renal cysts that measure (from top to bottom) 25, 15, and 7 mm. Gray content of body phantom, left kidney phantom, and cyst phantoms represent water. White content of right kidney phantom represents dilute contrast medium designed to have attenuation corresponding with that of nephrographic phase.

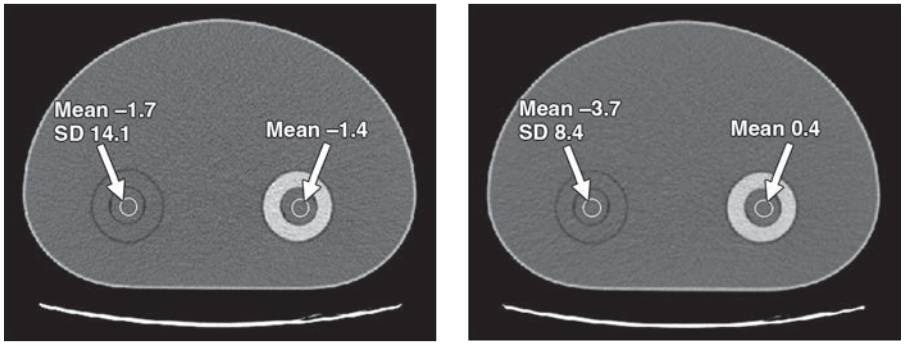

Fig. 3—Axial ultra-high-resolution CT (UHRCT) images of phantom reconstructed using 512 × 512 matrix and 3-mm slice thickness. Gray content of phantom represents water (unenhanced phase); white content of phantom represents dilute contrast medium designed to have attenuation corresponding with that of nephrographic phase.
A and **B,** Images acquired using UHRCT detector element sizes of 0.25 mm (**A**) and 0.5 mm (**B**) show ROIs (*arrows*) placed to evaluate cysts. Attenuation is recorded for both unenhanced and nephrographic phases, and SD is recorded for unenhanced phase as measure of image noise. Attenuation increase is 0.3 HU for detector element size of 0.25 mm and 4.1 HU for detector element size of 0.5 mm. Image noise is 14.1 HU for detector element size of 0.25 mm and 8.4 HU for detector element size of 0.5 mm.

TABLE 1: Effect of Detector Element Size on Attenuation Increase and Image Noise Stratified by Cyst Size in the Phantom Experiment

Detector Element (mm)	Attenuation Increase (HU)	*p*[a]	Image Noise (HU)	*p*[a]
With 25-mm cyst		**.02**		**.005**
0.5 Detector	3.8 ± 1.2		9.1 ± 1.2	
0.25 Detector	2.3 ± 1.4		14.4 ± 0.4	
With 15-mm cyst		**.03**		**.005**
0.5 Detector	6.8 ± 2.9		8.8 ± 1.3	
0.25 Detector	4.6 ± 2.7		14.2 ± 2.6	
With 7-mm cyst		.72		**.005**
0.5 Detector	5.3 ± 2.7		8.5 ± 1.5	
0.25 Detector	4.4 ± 4.1		13.2 ± 2.6	

Note—Unless otherwise noted, all values are expressed as mean ± SD. All images obtained using ultra-high-resolution CT, 512 × 512 matrix, 3-mm slice thickness, and hybrid iterative reconstruction.
[a]Comparison performed using Wilcoxon signed rank test. Listed in bold when statistically significant at $p < .05$.

was not significantly different between matrix sizes of 512 × 512 and 1024 × 1024 for any cyst size (all $p > .05$). Image noise was significantly greater for the 1024 × 1024 matrix than for the 512 × 512 matrix for the 15-mm cyst (16.2 ± 2.5 HU vs 14.2 ± 2.6 HU, $p = .005$) and 25-mm cyst (15.8 ± 0.5 HU vs 14.4 ± 0.4 HU, $p = .005$) but not for the 7-mm cyst ($p = .72$).

Slice thickness—Tables 3 and S3 (Table S3 is available in the online supplement) summarize the comparisons between slice thicknesses in the phantom experiment. Attenuation increase was not significantly associated with slice thickness for any of the three cysts (all $p > .05$). Image noise showed significant increases with decreasing slice thickness for all cyst sizes (all $p < .001$). For example, image noise at a slice thickness of 0.25 mm versus 3 mm was 20.4 ± 2.5 HU versus 13.2 ± 2.6 HU for the 7-mm cyst ($p < .001$), 21.8 ± 1.1 HU versus 14.2 ± 2.6 HU for the 15-mm cyst ($p < .001$), and 21.9 ± 1.1 HU versus 14.4 ± 0.4 HU for the 25-mm cyst ($p < .001$).

Clinical Study

Figure S2 (available in the online supplement) shows the Bland-Altman plots for assessing interreader agreement for the mean attenuation increase for each unique combination of parameters in the clinical study. The mean difference between readers for attenuation increase was –0.4 HU for a detector element size, matrix size, and slice thickness of 0.25 mm, 512 × 512, and 0.25 mm; –1.2 HU for 0.25 mm, 512 × 512, and 0.5 mm; –1.4 HU for 0.25 mm, 512 × 512, and 2 mm; –0.9 HU for 0.25 mm, 512 × 512, and 3 mm; –0.6 HU for 0.25 mm, 512 × 512, and 5 mm; and 0.9 HU for 0.25 mm, 1024 × 1024, and 3 mm.

TABLE 2: Effect of Matrix Size on Attenuation Increase and Image Noise Stratified by Cyst Size in the Phantom Experiment

Matrix Size	Attenuation Increase (HU)	*p*[a]	Image Noise (HU)	*p*[a]
With 25-mm cyst		.72		**.005**
512 × 512	2.3 ± 1.4		14.4 ± 0.4	
1024 × 1024	2.3 ± 1.4		15.8 ± 0.5	
With 15-mm cyst		.72		**.005**
512 × 512	4.6 ± 2.7		14.2 ± 2.6	
1024 × 1024	5.1 ± 2.2		16.2 ± 2.5	
With 7-mm cyst		.29		.72
512 × 512	4.4 ± 4.1		13.2 ± 2.6	
1024 × 1024	5.3 ± 4.2		13.1 ± 2.9	

Note—Unless otherwise noted, all values are expressed as mean ± SD. All images obtained using ultra-high-resolution CT, 0.25-mm detector element, 3-mm slice thickness, and hybrid iterative reconstruction.
[a]Comparison performed using Wilcoxon signed rank test. Listed in bold when statistically significant at $p < .05$.

TABLE 3: Effect of Slice Thickness on Attenuation Increase and Image Noise Stratified by Cyst Size in the Phantom Experiment

Slice Thickness (mm)	Attenuation Increase (HU)	*p*[a]	Image Noise (HU)	*p*[a]
With 25-mm cyst		.68		**< .001**
5	1.7 ± 0.8		11.4 ± 0.8	
3	2.3 ± 1.4		14.4 ± 0.4	
2	1.3 ± 1.2		15.7 ± 0.6	
0.5	1.7 ± 1.5		21.3 ± 1.2	
0.25	1.3 ± 1.5		21.9 ± 1.1	
With 15-mm cyst		.68		**< .001**
5	5.3 ± 1.9		11.6 ± 1.3	
3	4.6 ± 2.7		14.2 ± 2.6	
2	4.1 ± 2.4		16.4 ± 1.4	
0.5	4.7 ± 3.6		22.1 ± 1.8	
0.25	3.8 ± 3.2		21.8 ± 1.1	
With 7-mm cyst[b]		.39		**< .001**
3	4.4 ± 4.1		13.2 ± 2.6	
2	8.3 ± 6.5		14.9 ± 2.7	
0.5	8.9 ± 6.4		19.8 ± 3.6	
0.25	10.0 ± 6.8		20.4 ± 2.5	

Note—Unless otherwise noted, all values are expressed as mean ± SD. All images obtained using ultra-high-resolution CT, 0.25-mm detector element, 512 × 512 matrix, and hybrid iterative reconstruction.
[a]Comparison performed using Friedman test. Listed in bold when statistically significant at $p < .05$.
[b]Five-millimeter slice thickness not evaluated at this cyst size because of anticipated marked partial-volume effect, impacting attenuation measurements.

Patient characteristics—Height and weight information were available for 35 of the 36 patients. For these 35 patients, the mean height was 158.3 ± 7.7 cm (range, 141.5–173.5 cm), mean weight was 59.1 ± 8.2 kg (range, 42.4–74.7 kg), and mean BMI was 23.6 ± 2.6 (range, 17.8–28.7). The 118 cysts in the 36 patients comprised 36 cysts measuring less than 5 mm, 44 cysts measuring 5 mm and less than 10 mm, and 38 cysts measuring 10 mm and greater.

Matrix size—Table 4 summarizes the comparisons between matrix sizes in the clinical study. The mean attenuation increase was not significantly different between matrix sizes of 512 × 512 and 1024 × 1024 for any cyst size range (all $p > .05$). Among cysts smaller than 5 mm, the percentage of cysts showing pseudoenhancement of 10 HU and greater, 15 HU and greater, and 20 HU and greater was 66.7%, 63.9%, and 50.0%, respectively, for a matrix of 512 × 512 and 72.2%, 63.9%, and 58.3% for a matrix of 1024 × 1024.

TABLE 4: Effect of Matrix Size on Attenuation Increase and Image Noise Stratified by Cyst Size in the Clinical Study

Matrix Size	Attenuation Increase (HU)	p^a	Image Noise (HU)	p^a	Percentage of Cysts With Pseudoenhancement		
					≥ 10 HU	≥ 15 HU	≥ 20 HU
With cysts ≥ 10 mm		.68		**< .001**			
512 × 512	3.6 ± 4.9		13.2 ± 1.7		5.3 (2/38)	2.6 (1/38)	2.6 (1/38)
1024 × 1024	3.2 ± 4.7		14.3 ± 1.7		7.9 (3/38)	2.6 (1/38)	2.6 (1/38)
With cysts ≥ 5 to < 10 mm		.82		.22			
512 × 512	10.4 ± 10.0		13.7 ± 4.7		43.2 (19/44)	25.0 (11/44)	15.9 (7/44)
1024 × 1024	10.0 ± 9.9		14.8 ± 5.0		36.4 (16/44)	25.0 (11/44)	18.2 (8/44)
With cysts < 5 mm		.96		.98			
512 × 512	23.7 ± 22.5		12.3 ± 3.8		66.7 (24/36)	63.9 (23/36)	50.0 (18/36)
1024 × 1024	23.9 ± 22.1		12.4 ± 4.0		72.2 (26/36)	63.9 (23/36)	58.3 (21/36)

Note—Unless otherwise noted, all values are expressed as mean ± SD or percentage with raw data. All images obtained using ultra-high-resolution CT, 0.25-mm detector element, 3-mm slice thickness, and hybrid iterative reconstruction.

[a]Comparison performed using mixed-effect model. Listed in bold when statistically significant at $p < .05$.

Among cysts between 5 mm and less than 10 mm, the percentage of cysts showing pseudoenhancement of 10 HU and greater, 15 HU and greater, and 20 HU and greater was 43.2%, 25.0%, and 15.9%, respectively, for a matrix of 512 × 512 and 36.4%, 25.0%, and 18.2% for a matrix of 1024 × 1024. Among cysts 10 mm and greater, the percentage of cysts showing pseudoenhancement of 10 HU and greater, 15 HU and greater, and 20 HU and greater was 5.3%, 2.6%, and 2.6%, respectively, for a matrix of 512 × 512 and 7.9%, 2.6%, and 2.6% for a matrix of 1024 × 1024. Image noise for cysts 10 mm and greater was significantly greater for a 1024 × 1024 than a 512 × 512 matrix (14.3 ± 1.7 HU vs 13.2 ± 1.7 HU, $p < .001$). Otherwise, image noise was not significantly different between matrix sizes for the other cyst size ranges (all $p > .05$).

Slice thickness—Tables 5 and S3 show the comparisons among slice thicknesses in the clinical study. For cysts between 5 mm and less than 10 mm and cysts 10 mm and greater, mean attenuation increase was not significantly associated with slice thickness (both $p > .05$). For cysts smaller than 5 mm, attenuation increase showed a significant decrease with decreasing slice thickness, though there was no significant difference between 0.5-mm and 0.25-mm (23.7 ± 22.5 HU at 3 mm, 20.2 ± 22.7 HU at 2 mm, 11.6 ± 17.5 HU at 0.5 mm, and 12.6 ± 19.7 HU at 0.25 mm; $p < .001$); all pairwise comparisons were statistically significant ($p < .05$) aside from the comparisons of slice thicknesses of 2 mm versus 3 mm and of 0.25 mm versus 0.5 mm. Among cysts smaller than 5 mm, the percentage of cysts showing pseudoenhancement of 10 HU and greater, 15 HU and greater, and 20 HU and greater was 50.0%, 38.9%, and 36.1%, respectively, for a slice thickness of 0.25 mm, and 66.7%, 63.9%, and 50.0% for a slice thickness of 3 mm. Among cysts between 5 mm and less than 10 mm, the percentage of cysts showing pseudoenhancement of 10 HU and greater, 15 HU and greater, and 20 HU and greater was 34.1%, 15.9%, and 9.1%, respectively, for slice thickness of 0.25 mm and 43.2%, 25.0%, and 15.9% for a slice thickness of 3 mm. Among cysts 10 mm and greater, the percentage of cysts showing pseudoenhancement of 10 HU and greater, 15 HU and greater, and 20 HU and greater was 10.5%, 5.3%, and 0.0%, respectively, for a slice thickness of 0.25 mm and 5.3%, 2.6%, and 2.6% for a slice thickness of 3 mm. Image noise showed significant increases with decreasing slice thickness for all cyst size ranges (all $p < .001$). For example, image noise at a slice thickness of 0.25 mm versus at 3 mm was 17.2 ± 4.3 HU versus 12.3 ± 3.8 HU for cysts smaller than 5 mm, 19.7 ± 5.0 HU versus 13.7 ± 4.7 HU for cysts between 5 mm and less than 10 mm, and 20.5 ± 1.9 HU versus 13.2 ± 1.7 HU for cysts 10 mm and greater.

Discussion

This study represents the first to our knowledge to investigate renal cyst pseudoenhancement using UHRCT. Our study yields three important results. First, the phantom experiment suggests that the smaller detector element size of 0.25 mm (available for UHRCT in SHR mode but not available for conventional MDCT) may help reduce renal cyst pseudoenhancement in comparison with a detector element size of 0.5 mm. Second, an increased matrix size of 1024 × 1024 (available for UHRCT in SHR mode but not available for conventional MDCT) did not impact pseudoenhancement in comparison with a matrix size of 512 × 512 in the phantom experiment or clinical study. Third, the use of very thin slices (e.g., 0.25 or 0.5 mm, facilitated by UHRCT in SHR mode) resulted in reduced pseudoenhancement for cysts smaller than 5 mm in the clinical study. The findings indicate a possible role for UHRCT to reduce potential misinterpretation of small cystic renal lesions encountered on CT.

Pseudoenhancement consistently increased at smaller cyst sizes, corresponding with results from prior studies [11, 24]. Indeed, in the clinical study, a considerable percentage of cysts smaller than 5 mm and those between 5 mm and less than 10 mm showed pseudoenhancement of 10 HU and greater. Prior work indicates that a range of additional phenomena, including beam-hardening effect, partial-volume effect, and photoelectric effect, may also impact pseudoenhancement [6, 9, 11, 13, 20, 24, 25]. Thus, CT parameters impacting these phenomena could in turn affect the likelihood of pseudoenhancement at a given cyst size, as we have systematically evaluated in the present analysis.

TABLE 5: Effect of Slice Thickness on Attenuation Increase and Image Noise Stratified by Cyst Size in the Clinical Study

Slice Thickness (mm)	Attenuation Increase (HU)	*p*[a]	Image Noise (HU)	*p*[a]	Percentage of Cysts with Pseudoenhancement		
					≥ 10 HU	≥ 15 HU	≥ 20 HU
With cysts ≥ 10 mm		.99		**< .001**			
5	3.2 ± 4.9		11.0 ± 1.7		10.5 (4/38)	2.6 (1/38)	2.6 (1/38)
3	3.6 ± 4.9		13.2 ± 1.7		5.3 (2/38)	2.6 (1/38)	2.6 (1/38)
2	3.2 ± 5.2		15.3 ± 2.1		7.9 (3/38)	2.6 (1/38)	2.6 (1/38)
0.5	3.5 ± 5.2		20.0 ± 2.0		10.5 (4/38)	5.3 (2/38)	2.6 (1/38)
0.25	3.2 ± 5.3		20.5 ± 1.9		10.5 (4/38)	5.3 (2/38)	0.0 (0/38)
With cysts ≥ 5 to < 10 mm[b]		.70		**< .001**			
3	10.4 ± 10.0		13.7 ± 4.7		43.2 (19/44)	25.0 (11/44)	15.9 (7/44)
2	9.5 ± 9.2		15.6 ± 4.6		40.9 (18/44)	22.7 (10/44)	9.1 (4/44)
0.5	8.9 ± 9.8		19.6 ± 4.8		36.4 (16/44)	11.4 (5/44)	9.1 (4/44)
0.25	8.7 ± 9.8		19.7 ± 5.0		34.1 (15/44)	15.9 (7/44)	9.1 (4/44)
With cysts < 5 mm[b]		**< .001**		**< .001**			
3	23.7 ± 22.5		12.3 ± 3.8		66.7 (24/36)	63.9 (23/36)	50.0 (18/36)
2	20.2 ± 22.7		13.3 ± 3.6		66.7 (24/36)	63.9 (23/36)	41.7 (15/36)
0.5	11.6 ± 17.5		17.1 ± 4.1		52.8 (19/36)	44.4 (16/36)	27.8 (10/36)
0.25	12.6 ± 19.7		17.2 ± 4.3		50.0 (18/36)	38.9 (14/36)	36.1 (13/36)

Note—Unless otherwise noted, all values are expressed as mean ± SD or percentage with raw data. All images obtained using ultra-high-resolution CT, 0.25-mm detector element, 512 × 512 matrix, and hybrid iterative reconstruction.

[a]Comparison performed using mixed-effect model. Listed in bold when statistically significant at $p < .05$.

[b]Five-millimeter slice thickness not evaluated at this cyst size range because of anticipated marked partial-volume effect, impacting attenuation measurements.

The potential benefit of a smaller detector element size in reducing pseudoenhancement is a result of the significantly smaller attenuation increase observed at the smaller detector element size in the 15- and 25-mm cysts in the phantom experiment. Detector element size could not be evaluated in the clinical study given that only a single acquisition was performed at each phase in the patient scans and detector element size cannot be modified retrospectively. The reason for a potential impact of detector element size on pseudoenhancement is unclear. A prior phantom study of UHRCT reported higher effective energy for the 0.5-mm than the 0.25-mm detector element at an FOV of 350 mm [27]. This finding suggests that the 0.25-mm detector element is more affected by the beam-hardening effect than the 0.5-mm detector element, which would be expected to lead to more pronounced pseudoenhancement for the 0.25-mm detector element. On the other hand, our present observation of a smaller attenuation increase in the phantom for the 0.25-mm detector element may reflect a greater impact on attenuation increase by partial-volume effect (which would be reduced at the smaller detector element size) than by effective energy. Nonetheless, although the difference in attenuation increase between detector element sizes was statistically significant, the difference was small. Further studies remain warranted to better understand the impact of detector element size in renal lesion characterization in clinical settings.

In the clinical study, for cysts smaller than 5 mm, very thin slices resulted in reduced pseudoenhancement (i.e., 0.25- or 0.5-mm slice thickness in comparison with 3- or 5-mm slice thickness). In addition to a smaller mean attenuation increase, the percentage of cysts smaller than 5 mm showing clinically significant pseudoenhancement was also decreased at the very thin slice thicknesses. The decrease in pseudoenhancement for the very thin slices may reflect a decrease in partial-volume effect.

The decrease in detector element size, increase in matrix size, and decrease in slice thickness all resulted in increased image noise, consistent with prior studies [16, 17, 28]. Moreover, thinner slices are known to show noise-related degradation, which affects image quality [18, 19]. According to our analysis, noise does not appear to directly impact pseudoenhancement (e.g., no change in pseudoenhancement at different matrix sizes despite significant variation in noise). However, the increase in noise could nonetheless affect renal lesion characterization. According to the Bosniak classification version 2019 [29], renal masses can be characterized as Bosniak II cysts if they show homogeneous low attenuation. It may be argued that masses showing these features could be characterized as benign cysts regardless of the presence of pseudoenhancement, yet increased image noise may influence radiologists' subjective assessment of lesion homogeneity. Therefore, a parameter adjustment that results in reduced pseudoenhancement (thereby facilitating characterization of the lesion as a cyst) could have the trade-off of increased noise with associated apparent heterogeneity (thereby creating challenge in characterization as a cyst). All reconstructions in the current

study used hybrid iterative reconstruction, which reduces image noise and leads to a smoother image appearance, thus possibly counteracting the increased noise resulting from the explored parameter adjustments [12]. Although we documented objective image noise in the present analysis, subjective lesion homogeneity was not evaluated and warrants further investigation.

Our findings suggest a possibility for UHRCT when performing a multiphase renal-mass protocol to characterize an indeterminate renal mass. UHRCT would appear most likely to be helpful for small masses suspected to be cysts, representing the context in which pseudoenhancement is most likely to be relevant. When performing UHRCT in this context, consideration should be given to using the small detector element size (0.25 mm) and very thin slices (0.25 or 0.5 mm) to potentially reduce pseudoenhancement. However, a larger matrix size (1024 × 1024) would not be warranted for purposes of characterizing the renal lesion given the lack of an impact on pseudoenhancement yet increased image noise.

Our study has limitations. First, the clinical study was performed retrospectively at a single center with a small sample size and was thus prone to selection bias. Second, in the clinical study, pseudoenhancement could not be directly compared between distinct UHRCT and MDCT systems. The two systems could be compared through a prospective study in which patients undergo scans using both systems, although such an approach would entail patients receiving additional radiation exposure and contrast media injection for the second scan. Third, findings regarding the impact of detector element size remain speculative, given that detector element size was evaluated only in the phantom experiment. Fourth, all reconstructions were performed using hybrid iterative reconstruction; UHRCT reconstructed with filtered back projection was not evaluated. Finally, only lesions meeting a priori criteria for cysts were evaluated; the impact of UHRCT using the various parameter combinations on the detection of true enhancement by solid masses was not assessed.

In conclusion, this phantom experiment and clinical study suggest a possible role for UHRCT in reducing renal cyst pseudoenhancement through use of a smaller detector element size of 0.25 mm and, for cysts smaller than 5 mm, through generation of very thin slices of 0.25 or 0.5 mm. However, the smaller detector element size and the very thin slices resulted in increased image noise. An increased matrix of 1024 × 1024 did not impact pseudoenhancement. Although requiring further evaluation in clinical contexts, the findings raise the possibility that UHRCT could facilitate the characterization of small cystic renal lesions, thereby reducing equivocal or inaccurate interpretations and avoiding inappropriate or unnecessary follow-up recommendations.

Acknowledgments

We thank Kenta Matsuda and Takuto Noguchi for their valuable support with image collection, Kazuya Minamishima and Yoshiki Owaki (Office of Radiological Technology, Keio University Hospital) and Koichi Sugisawa (e Medical Tokyo Co., Ltd.) for allowing the use of their phantom, and Naoki Edo (Division of Behavioral Science, National Defense Medical College Research Institute) and Takahiro Nakamura (Department of Mathematics, National Defense Medical College) for their assistance with statistical analysis in this study.

References

1. Jinzaki M, McTavish JD, Zou KH, Judy PF, Silverman SG. Evaluation of small (≤ 3 cm) renal masses with MDCT: benefits of thin overlapping reconstructions. *AJR* 2004; 183:223–228
2. Israel GM, Bosniak MA. How I do it: evaluating renal masses. *Radiology* 2005; 236:441–450
3. Silverman SG, Israel GM, Trinh QD. Incompletely characterized incidental renal masses: emerging data support conservative management. *Radiology* 2015; 275:28–42
4. Hindman NM. Approach to very small (< 1.5 cm) cystic renal lesions: ignore, observe, or treat? *AJR* 2015; 204:1182–1189
5. Curry NS, Cochran ST, Bissada NK. Cystic renal masses: accurate Bosniak classification requires adequate renal CT. *AJR* 2000; 175:339–342
6. Birnbaum BA, Maki DD, Chakraborty DP, Jacobs JE, Babb JS. Renal cyst pseudoenhancement: evaluation with an anthropomorphic body CT phantom. *Radiology* 2002; 225:83–90
7. Heneghan JP, Spielmann AL, Sheafor DH, Kliewer MA, DeLong DM, Nelson RC. Pseudoenhancement of simple renal cysts: a comparison of single and multidetector helical CT. *J Comput Assist Tomogr* 2002; 26:90–94
8. Maki DD, Birnbaum BA, Chakraborty DP, Jacobs JE, Carvalho BM, Herman GT. Renal cyst pseudoenhancement: beam-hardening effects on CT numbers. *Radiology* 1999; 213:468–472
9. Coulam CH, Sheafor DH, Leder RA, Paulson EK, DeLong DM, Nelson RC. Evaluation of pseudoenhancement of renal cysts during contrast-enhanced CT. *AJR* 2000; 174:493–498
10. Abdulla C, Kalra MK, Saini S, et al. Pseudoenhancement of simulated renal cysts in a phantom using different multidetector CT scanners. *AJR* 2002; 179:1473–1476
11. Tappouni R, Kissane J, Sarwani N, Lehman EB. Pseudoenhancement of renal cysts: influence of lesion size, lesion location, slice thickness, and number of MDCT detectors. *AJR* 2012; 198:133–137
12. Krishna S, Murray CA, McInnes MD, et al. CT imaging of solid renal masses: pitfalls and solutions. *Clin Radiol* 2017; 72:708–721
13. Birnbaum BA, Hindman N, Lee J, Babb JS. Renal cyst pseudoenhancement: influence of multidetector CT reconstruction algorithm and scanner type in phantom model. *Radiology* 2007; 244:767–775
14. Yanagawa M, Hata A, Honda O, et al. Subjective and objective comparisons of image quality between ultra-high-resolution CT and conventional area detector CT in phantoms and cadaveric human lungs. *Eur Radiol* 2018; 28:5060–5068
15. Kakinuma R, Moriyama N, Muramatsu Y, et al. Ultra-high-resolution computed tomography of the lung: image quality of a prototype scanner. *PLoS One* 2015; 10:e0137165
16. Hata A, Yanagawa M, Honda O, et al. Effect of matrix size on the image quality of ultra-high-resolution CT of the lung: comparison of 512 ×512, 1024 × 1024, and 2048 × 2048. *Acad Radiol* 2018; 25:869–876
17. Akagi M, Nakamura Y, Higaki T, et al. Deep learning reconstruction improves image quality of abdominal ultra-high-resolution CT. *Eur Radiol* 2019; 29:6163–6171
18. Tamm EP, Rong XJ, Cody DD, Ernst RD, Fitzgerald NE, Kundra V. Quality initiatives: CT radiation dose reduction: how to implement change without sacrificing diagnostic quality. *RadioGraphics* 2011; 31:1823–1832
19. Kanal KM, Stewart BK, Kolokythas O, Shuman WP. Impact of operator-selected image noise index and reconstruction slice thickness on patient radiation dose in 64-MDCT. *AJR* 2007; 189:219–225
20. Wang ZJ, Coakley FV, Fu Y, et al. Renal cyst pseudoenhancement at multidetector CT: what are the effects of number of detectors and peak tube voltage? *Radiology* 2008; 248:910–916
21. Sugisawa K, Ichikawa K, Minamishima K, Hasegawa M, Yamada Y, Jinzaki M.

Evaluation of the CT parameters to suppress renal cysts pseudoenhancement effect: influence of the virtual monochromatic spectral images, the model-based iterative reconstruction algorithm and the aperture size in phantom model [in Japanese]. *Nippon Hoshasen Gijutsu Gakkai Zasshi* 2017; 73:636–645

22. Yamada Y, Yamada M, Sugisawa K, et al. Renal cyst pseudoenhancement: intraindividual comparison between virtual monochromatic spectral images and conventional polychromatic 120-kVp images obtained during the same CT examination and comparisons among images reconstructed using filtered back projection, adaptive statistical iterative reconstruction, and model-based iterative reconstruction. *Medicine (Baltimore)* 2015; 94:e754
23. Mileto A, Nelson RC, Samei E, et al. Impact of dual-energy multi-detector row CT with virtual monochromatic imaging on renal cyst pseudoenhancement: in vitro and in vivo study. *Radiology* 2014; 272:767–776
24. Bae KT, Heiken JP, Siegel CL, Bennett HF. Renal cysts: is attenuation artifactually increased on contrast-enhanced CT images? *Radiology* 2000; 216:792–796
25. Sai V, Rakow-Penner R, Yeh BM, et al. Renal cyst pseudoenhancement at 16- and 64-dector row MDCT. *Clin Imaging* 2013; 37:520–525
26. Suh M, Coakley FV, Qayyum A, Yeh BM, Breiman RS, Lu Y. Distinction of renal cell carcinomas from high-attenuation renal cysts at portal venous phase contrast-enhanced CT. *Radiology* 2003; 228:330–334
27. Muramatsu S, Kayano S, Sato K. Evaluation of x-ray beam quality in different bowtie filters on ultra-high resolution CT [in Japanese]. *Jpn J Comput Tomogr Technol* 2020; 8:1
28. Monnin P, Sfameni N, Gianoli A, Ding S. Optimal slice thickness for object detection with longitudinal partial volume effects in computed tomography. *J Appl Clin Med Phys* 2017; 18:251–259
29. Silverman SG, Pedrosa I, Ellis JH, et al. Bosniak classification of cystic renal masses, version 2019: an update proposal and needs assessment. *Radiology* 2019; 292:475–488

Editorial Comment: Pseudoenhancement—New Solutions to Old Problems?

Pseudoenhancement, or the artifactual increase in attenuation on contrast-enhanced CT, confounds evaluation of renal masses, especially small endophytic masses. In 20% of simple renal cysts, pseudoenhancement can result in spurious attenuation increase by 10 HU or more. Pseudoenhancement may result in increased follow-up imaging or overtreatment of benign cysts. To account for pseudoenhancement, the Bosniak classification version 2019 revised the threshold for benignity (classes I and II) in homogeneous masses on contrast-enhanced CT to 30 HU (vs 20 HU threshold on noncontrast CT) [1]. Nonetheless, identifying the source of pseudoenhancement and completely eliminating it remains desirable given incidental renal cysts' high prevalence.

In their original description in 1999, Maki et al. [2] speculated that pseudoenhancement was likely a result of inadequate beam-hardening correction and would likely be fixed by a reconstruction modification. However, optimism quickly waned because pseudoenhancement continued to be reported despite changes in CT hardware and reconstruction algorithms. Furthermore, for MDCT, prevalence of pseudoenhancement increased with an increasing number of detector arrays. More recently, dual-energy CT has shown promise in eliminating the polychromatic source of beam hardening by generating virtual monoenergetic images [3].

In this study, the authors evaluate ultra-high-resolution CT, showing in a phantom that a small detector element size of 0.25 mm mitigated pseudoenhancement compared with a conventional detector size of 0.5 mm. This benefit was not present in 7-mm cysts and not tested in patients, and further verification is necessary. Also, for cysts smaller than 5 mm in patients, thinner slice thickness reduced pseudoenhancement compared with a standard 3-mm slice thickness; this difference was at the expense of increased image noise. Thus, pseudoenhancement is likely multifactorial and may require multiple approaches. Until solutions that completely eliminate pseudoenhancement are found, the only recourse is to be educated, recognize the problem, and use modified renal cyst definitions to account for pseudoenhancement.

Satheesh Krishna, MD
University of Toronto
Toronto General Hospital
Toronto, ON, Canada
satheeshkrishna.jeyaraj@utoronto.ca

The author declares that there are no disclosures relevant to the subject matter of this article.

doi.org/10.2214/AJR.22.28037

References

1. Silverman SG, Pedrosa I, Ellis JH, et al. Bosniak classification of cystic renal masses, version 2019: an update proposal and needs assessment. *Radiology* 2019; 292:475–488
2. Maki DD, Birnbaum BA, Chakraborty DP, Jacobs JE, Carvalho BM, Herman GT. Renal cyst pseudoenhancement: beam-hardening effects on CT numbers. *Radiology* 1999; 213:468–472
3. Mileto A, Nelson RC, Samei E, et al. Impact of dual-energy multi-detector row CT with virtual monochromatic imaging on renal cyst pseudoenhancement: in vitro and in vivo study. *Radiology* 2014; 272:767–776